Nanometre-scale germanium photodetector enhanced by a near-infrared dipole antenna

LIANG TANG[1]*, SUKRU EKIN KOCABAS[1], SALMAN LATIF[1], ALI K. OKYAY[2], DANY-SEBASTIEN LY-GAGNON[1], KRISHNA C. SARASWAT[2] AND DAVID A. B. MILLER[1]

[1]Ginzton Laboratory, Stanford University, Stanford, California 94305, USA
[2]Center for Integrated Systems, Stanford University, Stanford, California 94305, USA
*e-mail: luke_tang@stanford.edu

A critical challenge for the convergence of optics and electronics is that the micrometre scale of optics is significantly larger than the nanometre scale of modern electronic devices. In the conversion from photons to electrons by photodetectors, this size incompatibility often leads to substantial penalties in power dissipation, area, latency and noise[1–4]. A photodetector can be made smaller by using a subwavelength active region; however, this can result in very low responsivity because of the diffraction limit of the light. Here we exploit the idea of a half-wave Hertz dipole antenna (length $\sim$ 380 nm) from radio waves, but at near-infrared wavelengths (length $\sim$ 1.3 μm), to concentrate radiation into a nanometre-scale germanium photodetector. This gives a polarization contrast of a factor of 20 in the resulting photocurrent in the subwavelength germanium element, which has an active volume of 0.00072 μm^3, a size that is two orders of magnitude smaller than previously demonstrated detectors at such wavelengths.

The interaction of light with nanostructured metals has been studied extensively in recent years[5–10]. The resulting near-field optical intensity can be two to three orders of magnitude higher than the incident intensity. However, very little research has been carried out into the interaction of these strong near fields with semiconductors and the further transformation of the optical energy into electricity[11–13]. It has recently been demonstrated that the photogeneration of carriers in silicon can be enhanced by a surface-plasmon antenna at a wavelength of 840 nm (ref. 12). This method has the practical limitation that the entire grating structure necessary for exciting a surface-plasmon resonance occupies a large area in terms of wavelengths. Alternatively, a C-shaped aperture has been used to enhance photodetection locally without exciting long-range surface-plasmon resonances[13]. However, for easy integration and high-speed, low-capacitance operation, it is generally advantageous to design planar devices such as the metal–semiconductor–metal (MSM) detectors that are widely used in high-speed optical receivers[14].

Resonant antennas can confine strong optical near fields in a subwavelength volume, as demonstrated recently for bow-tie antennas and dipole antennas at visible wavelengths using the resulting scattered light[15,16]. The optical properties of the structures largely depend on the size and shape of the antennas.
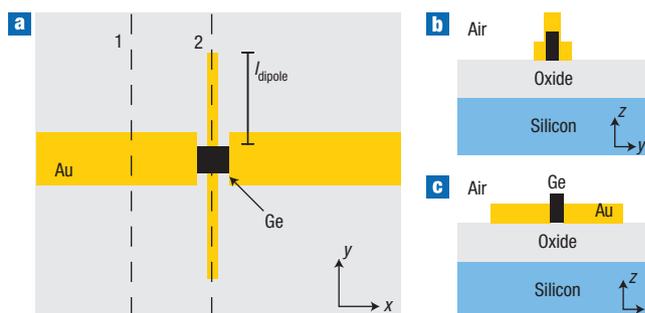
Figure 1 A schematic of the device. a, Top view of the open-sleeve dipole antenna consisting of a dipole antenna oriented in the *y* direction and two line electrodes (sleeves) in the *x* direction. **b**, Cross-section of the germanium nanowire (through line 1 in panel **a**) lying under the two line electrodes. **c**, Cross-section (corresponding to line 2 in panel **a**) showing germanium in the gap region between the two antenna arms.

Using the principle of high field enhancement by an antenna, we present a deeply subwavelength MSM photodetector. Figure 1 shows a schematic of the device structure. The open-sleeve dipole antenna made of gold consists of a dipole oriented along the *y* direction and two line electrodes (sleeves) along the *x* direction. A germanium nanowire lies under the two line electrodes and in the gap region between the two dipole arms. Open-sleeve dipole antennas were initially proposed[17] for radio frequencies to increase the bandwidth of an ordinary dipole antenna. In our device, the dipole was used to collect light from a large area and concentrate it into the small subwavelength region of the germanium. The sleeves were used to extract photocurrent without substantially changing the antenna characteristics (from a bare dipole). Crystalline germanium was chosen to be the active material of our photodetector because of its high responsivity at near-infrared wavelengths and its compatibility with standard silicon technology[18]. Previous research has shown that use of a substrate with a high dielectric constant significantly
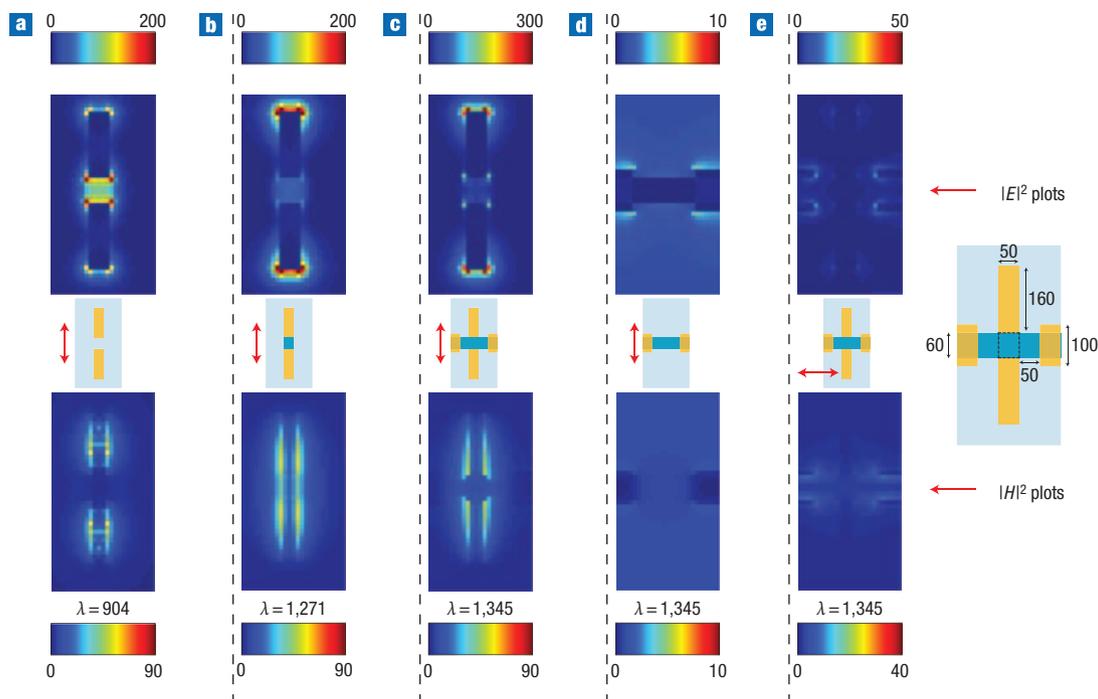
Figure 2 FDTD-simulated optical near-field intensity 25 nm above the substrate surface. The top row is the square of the E-field magnitude, and the bottom row is the square of the H-field magnitude. The diagrams and arrows in the middle row indicate the configuration and the polarization direction, respectively. **a–e**, The gold metal arms are all 50 nm wide, 50 nm thick and 160 nm long. The gap between the two metal arms is 60 nm. The substrate is SiO$_2$ ($n = 1.44$). Light is polarized parallel to the antenna arms except when otherwise stated. **a**, Dipole arms (no sleeves) with an air gap, resonant at 904 nm. **b**, Dipole arms (no sleeves), as in **a**, but with the gap filled with germanium, resonant at 1,271 nm. **c**, Open-sleeve dipole structure resonant at 1,345 nm. **d**, Open-sleeve dipole structure, as in **c**, but with no dipole arms. **e**, Open-sleeve dipole structure, as in **c**, but with light polarized perpendicular to the antenna arms. The colour scale bar refers to the enhancement ratio over the square of the corresponding incident-field magnitude; note that the colour scales are different for different plots.

weakens the antenna resonant strength[13]. To avoid this effect, our detector was fabricated on a thick oxide layer.

To understand the physics, we first studied several configurations using a finite-difference time-domain (FDTD) method (Fig. 2). In all configurations the metal arms were 50 nm wide, 50 nm thick and 160 nm long, and the gap between the two metal arms was 60 nm. The substrate was SiO$_2$ (with a refractive index, $n = 1.44$). In Fig. 2a, with air in the gap region, the structure was resonant at a wavelength of 904 nm with the highest electric (E-)field in the gap region. The magnetic (H-)field distribution (bottom row of Fig. 2) indicates that the two metal arms were weakly coupled[19,20] and each behaved approximately as a half-wave dipole. In Fig. 2b, with germanium filling the gap region, the structure was resonant at a wavelength of 1,271 nm. The H-field distribution indicates that the whole structure behaved approximately as a single half-wave dipole antenna. The high dielectric constant of germanium ($\varepsilon = 19$) probably induced the strong coupling between the two metal arms. Although with germanium in the gap the strongest fields were at the two ends of the antenna instead of in the middle gap, the highest energy was still concentrated in the gap owing to the high dielectric constant of germanium (the E-field energy density is proportional to ε times the plotted squared E-field magnitudes). The dipole length determines the main resonance of the antenna. Because of the properties of real metals at near-infrared frequencies and the effects of the substrate dielectric constant[21], the first resonant antenna length was substantially less than half of a free-space wavelength (half λ). The addition of the line electrodes laterally on either side of the gap only slightly

shifted the resonant wavelength, as shown in Fig. 2b,c. The germanium was 80 nm thick and the distance between the two line electrodes was 150 nm. The near-field distribution confirms that the line electrodes do not qualitatively affect the nature of the dipole antenna, consistent with the original proposal for the microwave sleeved dipole antenna[17]. Additionally, there was very little field enhancement in the arrangement with no antenna arms (Fig. 2d) or if the light was polarized perpendicular to the antenna arms (Fig. 2e). These simulations therefore confirm our expectation that this structure behaves essentially as a half-wave Hertz dipole antenna, concentrating the E-field in the high-dielectric-constant germanium in the gap region. The strong optical near field generates carriers within this small volume, which we expect is fully depleted by the lateral metal Schottky contacts. Therefore our antenna structure is qualitatively different from recent nanometallic gap antennas, such as those described in refs 15, 16 and 19. The high E-field at the two ends of the dipole antenna indicates a large effective capture area for the incident light, and the high H-field in the gap region shows the large effective current flow through the detector element, as required for the overall half-wavelength antenna behaviour and for strong detection in this near-infrared antenna receiver.
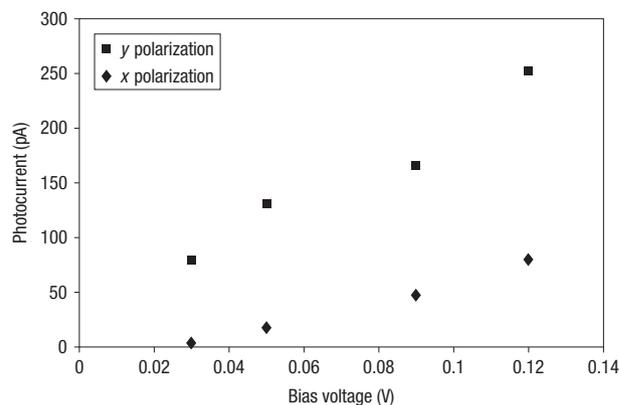
The detector active region in our device has a volume of ~150 nm × 60 nm × 80 nm, which we believe is the smallest semiconductor photodetector demonstrated experimentally so far. The nanoscale dimensions of the photodetector raise an experimental challenge—that is, fabricating both the antenna and the germanium element with sufficient precision and aligning them with each other. The challenge can be met by incorporating
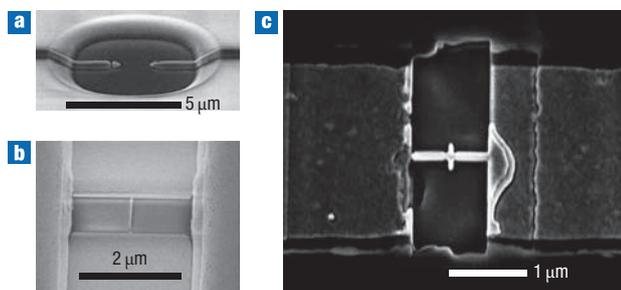
Figure 3 Scanning electron microscopy (SEM) images of the fabricated devices. **a**, Silicon seeding window with 2-μm-wide germanium crystalline lines. **b**, 60-nm-wide and 2-μm-long germanium nanowire fabricated by the first FIB step. **c**, An open-sleeve dipole antenna detector with $l_{dipole} = 155$ nm (this image is rotated by 90° in relation to that in **b**). (Charging due to a thick oxide layer limits the resolution in this SEM image.)

Figure 4 Bias voltage dependence of an antenna detector. The value of l_{dipole} is 155 nm for two orthogonal light polarizations at a wavelength of 1,310 nm. The photocurrent when the light polarization is parallel to the dipole antenna (*y* polarized) is about 20 times higher than when it is perpendicular to them (*x* polarized) at 0.03 V bias voltage.

two steps of focused-ion-beam (FIB) milling. First, 1-μm-thick SiO₂ was grown on silicon by oxidation at 1,100 °C and a silicon seeding window opened in the oxide. Then, 80-nm-thick amorphous germanium was deposited using low-pressure chemical vapour deposition, patterned and aligned to the silicon seeding window (Fig. 3a). A thin layer of low-temperature SiO₂ was deposited to encapsulate the patterned germanium lines. Rapid thermal annealing was used to heat the wafers up to 940 °C for 2 s to melt the germanium. Germanium crystalline growth started from the silicon (100)/germanium interface and propagated laterally through the germanium liquid on top of the oxide films[22]. After the oxide etch, germanium nanowires with a width of 60 nm and length 2 μm were fabricated using an FEI Strata DB 235 FIB tool (Fig. 3b). Titanium of 5 nm thickness and then gold of 45 nm thickness were deposited using electron-beam evaporation. The titanium layer was used to improve the adhesion of gold to the oxide. Metal layers were patterned and lifted off to form the electrical contacts. Finally, the open-sleeve dipole antennas were shaped from the metal layer by FIB (Fig. 3c).

The photocurrent from the detectors was measured using a lock-in amplifier with a modulation frequency up to 1.5 kHz. Light at a wavelength of 1,310 nm was incident on the detector. Photocurrent was collected from the two line electrodes oriented in the *x* direction. The laser spot was focused to about 3 μm in diameter. We measured the polarization dependence of the photocurrent by rotating a half-wave plate in the optical path. The photocurrent reached maxima when the light polarization was parallel to the dipole antenna (*y* polarized) and fell to minima when it was perpendicular to them (*x* polarized), as expected theoretically. The voltage bias dependence of photocurrent is shown in Fig. 4 for an antenna with an arm length $l_{dipole} = 155$ nm under 3 μW laser illumination. This responsivity is probably reduced substantially compared with that of perfect bulk germanium because of increased surface recombination and crystal defects resulting from Ga⁺ ions implanted in the FIB process; such phenomena and the observed variability of the overall responsivity between different similar devices make absolute measurements of the detector response unreliable. For a given device we can, however, compare the photocurrent in different polarizations, and we measured the photocurrent for *y*-polarized incident light to be 20 times that for *x*-polarized light at a very low bias voltage. This polarization-dependent signal of the photodetector is direct evidence of an
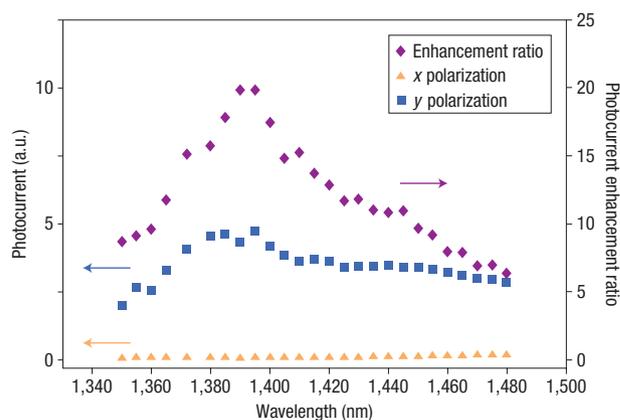
Figure 5 Measured photocurrent responses for light polarization in the *y* and *x* directions. The wavelengths were 1,350−1,480 nm for the detector with $l_{dipole} = 160$ nm.

antenna effect in the near infrared. At higher bias voltages, the enhancement is reduced to about a factor of three, possibly as a result of to the collection of additional carriers generated by light that leaks into the region under the line electrodes. As the fields in that region are not enhanced by the antenna, the resulting photocurrent may have less polarization dependence, and the average photocurrent enhancement would therefore be lower at higher bias voltages. This effect could potentially be avoided if the germanium under the electrodes was removed, leaving only that in the gap region. Although more precise alignment techniques in the nanofabrication process are required to achieve this objective, such alignment is within the current photolithography capability in the semiconductor industry.

We also measured the spectral response of a detector for *y*- and *x*-polarized light when the laser was tuned from 1,350 nm to 1,480 nm, with a bias voltage of 0.03 V, in a structure with antenna arm lengths of $l_{dipole} = 160$ nm (Fig. 5). The ratio between the two photocurrent values is plotted so as to factor out the spectral dependence of the germanium absorption

coefficient. The resonant peak at a wavelength of 1,390 nm is characteristic of half-wavelength antenna behaviour. This measured resonance is close to the designed resonant wavelength of 1,345 nm. The photodetector has a relatively wide bandwidth, and hence is potentially suitable for wavelength-division-multiplexing telecommunication applications.

FDTD calculations were performed for the near-field distribution of the detector at a wavelength of 1,390 nm. A volume integration of the E-field intensity was performed in the germanium active region to estimate photocurrent enhancement. The volume-integration value for y-polarized light was calculated to be 28 times that for x-polarized light. This theoretical polarization enhancement agrees well with our experimental observation. We also performed the calculation for the same germanium structure with sleeves but no dipole arms for y-polarized light. The volume-integration value for y polarization for the structure with dipole arms was about 70 times that for the structure without dipole arms. This suggests that the absolute photocurrent enhancement due to the dipole antenna may be even higher than the observed polarization enhancement ratio of 20.

The transit time of the carriers across the 150-nm-long depletion layer was calculated to be about 1.5 ps, and the cutoff frequency was estimated to be over 100 GHz, assuming the drift velocity of the carriers to be $\sim 1 \times 10^7$ cm s^{-1}. This rough estimate suggests the possibility of high-speed operation. With a junction area of 60 nm × 80 nm, the detector capacitance is estimated to be as small as ~ 0.005 fF (5 aF) based on the simple parallel-plate model. This extremely low capacitance would permit the use of a high load resistance to obtain a high output voltage at high frequencies, potentially enabling optoelectronic integrated circuits with very low optical and electrical power consumption.

In conclusion, we have experimentally demonstrated a germanium photodetector with an active volume on the order of $1 \times 10^{-4} \lambda^3$, using a Hertz dipole antenna at 1,310−1,480 nm wavelengths. We have also shown an enhancement by a factor of 20 in the relative photocurrent in the detector due to the antenna resonance, providing an efficient way to dramatically improve the sensitivity of subwavelength semiconductor photodetectors. The device shown here could serve to bridge the large gap between micrometre-scale dielectric photonic devices and nanometre-scale electronics.

References

1. Goodman, J. W., Leonberger, F. J., Kung S. Y. & Athale, R. A. Optical interconnections for VLSI systems. *Proc. IEEE* **72,** 850−866 (1984).
2. Miller, D. A. B. Rationale and challenges for optical interconnects to electronic chips. *Proc. IEEE* **88,** 728−749 (2000).
3. Meindl, J. D. *et al.* Interconnect opportunities for gigascale integration. *IBM Res. Dev.* **46,** 245−263 (2002).
4. Krishnamoorthy, A. V. & Miller, D. A. B. Scaling optoelectronic−VLSI circuits into the 21st century: A technology roadmap. *IEEE J. Sel. Top. Quant. Electron.* **2,** 55−76 (1996).
5. Ebbesen, T. W., Lezec, H. J., Ghaemi, H. F., Thio, T. & Wolff, P. A. Extraordinary optical transmission through sub-wavelength hole arrays. *Nature* **391,** 667−669 (1998).
6. Lezec, H. J. *et al.* Beaming light from a subwavelength aperture. *Science* **297,** 820−822 (2002).
7. Sanchez, E. J., Novotny, L. & Xie, X. S. Near field fluorescence microscopy based on two-photon excitation with metal tips. *Phys. Rev. Lett.* **82,** 4014−4017 (1999).
8. Fromm, D. P., Sundaramurthy, A., Schuck, P. J., Kino, G. & Moerner, W. E. Gap-dependent optical coupling of single bowtie nanoantennas resonant in the visible. *Nano Lett.* **4,** 957−961 (2004).
9. Bozhevolnyi, S. I., Volkov, V. S., Devaux, E., Laluet, J.-Y. & Ebbesen, T. W. Channel plasmon subwavelength waveguide components including interferometers and ring resonators. *Nature* **440,** 508−511 (2006).
10. Fumeaux, C., Alda, J. & Boreman, G. D. Lithographic antennas at visible frequencies. *Opt. Lett.* **24,** 1629−1631 (1999).
11. Schaadt, D. M., Feng, B. & Yu, E. T. Enhanced semiconductor optical absorption via surface plasmon excitation in metal nanoparticles. *Appl. Phys. Lett.* **86,** 063106 (2005).
12. Ishi, T., Fujikata, J., Makita, K., Baba, T. & Ohashi, K. Si nano-photodiode with a surface plasmon antenna. *Jpn J. Appl. Phys.* **44,** L364−L366 (2005).
13. Tang, L. *et al.* C-shaped nanoaperture-enhanced germanium photodetector. *Opt. Lett.* **31,** 1519−1521 (2006).
14. Chui, C. O., Okyay, A. K. & Saraswat, K. C. Effective dark current suppression with asymmetric MSM photodetectors in group IV semiconductors. *IEEE Photon. Technol. Lett.* **15,** 1585−1587 (2003).
15. Muhlschlegel, P., Eisler, H.-J., Martin, O. J. F., Hecht, B. & Pohl, D. W. Resonant optical antennas. *Science* **308,** 1607−1609 (2005).
16. Schuck, P. J., Fromm, D. P., Sundaramuthy, A., Kino, G. S. & Moerner, W. E. Improving the mismatch between light and nanoscale objectives with gold bowtie nanoantennas. *Phys. Rev. Lett.* **94,** 017402 (2005).
17. King, H. E. & Wong, J. L. An experimental study of a Balun-fed open-sleeve dipole in front of a metallic reflector. *IEEE Trans. Antennas Propagation* **AP-20,** 201−204 (1972).
18. Colace, L., Masini, G. & Assanto, G. Ge-on-Si approaches to the detection of near-infrared light. *IEEE J. Quant. Electron.* **35,** 1843−1852 (1999).
19. Cubukcu, E., Kort, E. A., Crozier, K. B. & Capasso, F. Plasmonic laser antenna. *Appl. Phys. Lett.* **89,** 093120 (2006).
20. Aizpurua, J., Bryant, G. W., Richter, L. J. & García de Abajo, F. J. Optical properties of coupled metallic nanorods for field-enhanced spectroscopy. *Phys. Rev. B* **71,** 235420 (2005).
21. Codreanu, I. & Boreman, G. D. Influence of dielectric substrate on the responsivity of microstrip dipole-antenna-coupled infrared microbolometers. *Appl. Opt.* **41,** 1835−1840 (2002).
22. Liu, Y. C., Deal, M. D. & Plummer, J. D. Rapid melt growth of germanium crystals with self-aligned microcrucibles on Si substrates. *J. Electrochem. Soc.* **152,** G688−G693 (2005).